

# Three material decomposition for spectral computed tomography enabled by block-diagonal step-preconditioning

Emil Y. Sidky<sup>1</sup>, Rina Foygel Barber<sup>2</sup>, Taly Gilat-Schmidt<sup>3</sup>, and Xiaochuan Pan<sup>1</sup>

**Abstract**—A potential application for spectral computed tomography (CT) with multi-energy-window photon-counting detectors is quantitative medical imaging with K-edge contrast agents [1]. Image reconstruction for spectral CT with such contrast agents necessitates expression of the X-ray linear attenuation map in at least three expansion functions, for example, bone/water/K-edge-material or photo-electric-process/Compton-process/K-edge-material. The use of three expansion functions can result in slow convergence for iterative image reconstruction (IIR) algorithms applied to spectral CT. We propose a block-diagonal step-preconditioner for use with a primal-dual iterative image reconstruction framework that we have been developing for spectral CT. We demonstrate the advantage of the new step-preconditioner on a sensitive spectral CT simulation where the test object has low concentration of Gadolinium (Gd) contrast agent and the X-ray attenuation map is represented by three materials - PMMA, a soft-tissue equivalent, Aluminum, a bone equivalent, and Gd.

## I. INTRODUCTION

We have been developing a general algorithm framework for one-step spectral CT image reconstruction (OSSCIR) that we have applied to experimental data acquired employing a spectral CT system with photon-counting detectors [2]. The OSSCIR algorithm framework involves direct one-step image reconstruction of basis material maps from energy-windowed X-ray transmission data. The one-step approach contrasts with standard two-step processing where the photon transmission data is converted to material sinograms followed by image reconstruction to material maps [1].

The one-step approach enables unconventional scan configurations where the transmission rays need not be co-registered for all energy-windows [3], and the image reconstruction process can be regularized by applying constraints directly to the material maps. Implementing OSSCIR consists of: (1) specifying the material maps with an optimization problem that includes a nonconvex data discrepancy term with convex constraints, and (2) solution of the nonconvex optimization problem by the mirrored convex/concave (MOCCA) algorithm [4,5].

MOCCA is the heart of the OSSCIR framework. It is an extension of the Chambolle-Pock primal-dual (CPPD) algorithm for large-scale convex optimization [6,7]. The MOCCA extension applies to certain forms of large-scale nonconvex optimization composed of a smooth nonconvex objective function and convex nonsmooth functions, such as convex constraints. The design of MOCCA is based on the idea that for some classes of nonconvex smooth objective functions the difficulty for algorithm design results from local saddle points and not local minima. Local saddle points have directions of negative curvature that can result in spurious update steps. Accordingly, a MOCCA iteration consists of constructing a local convex quadratic approximation to the objective function, removing directions of negative curvature, and performing a CPPD step on this approximation.

An important aspect of MOCCA is the diagonal step-preconditioner (SPC) for CPPD proposed by Pock and Chambolle [8]. Because the convex approximation to the objective function is changing at every iteration, the CPPD step length parameters need to be recomputed at every iteration. The step lengths of diagonal-SPC CPPD Ref. [8] can be computed at the cost of two additional matrix-vector product operations, which is equivalent to an additional forward- and back-projection per iteration for CT IIR.

<sup>1</sup>The University of Chicago, Department of Radiology MC-2026, 5841 S. Maryland Avenue, Chicago IL, 60637.

<sup>2</sup>The University of Chicago, Department of Statistics, 5734 S. University Avenue, Chicago IL, 60637.

<sup>3</sup>Marquette University, Department of Biomedical Engineering, PO Box 1881, Milwaukee WI, 53201.

In this contribution, we extend diagonal SPC to block-diagonal SPC that effectively counteracts slow convergence due to the near linear dependence from the basis material attenuation curves. In our original work on spectral CT IIR, we had already encountered slow convergence rates with two-material expansion of the attenuation map, and in that work we proposed  $\mu$ -preconditioning ( $\mu$ -PC), where the materials expansion set is transformed to an orthogonal set of functions in X-ray energy. The  $\mu$ -PC transformation was effective at improving convergence rates.

In attacking three-materials expansion sets,  $\mu$ -PC also improves convergence, but in this case the convergence issue is more acute than the two-materials case. In our original application of MOCCA to spectral CT in Ref. [5], we successfully demonstrated one-step reconstruction for three materials, but the simulation modeled five ideal photon-counting spectral response windows with sharp boundaries and no window overlap. The three-material simulation we consider here involves only four windows with realistic spectral responses that have significant overlap with each other. Accordingly, the worse conditioning of the realistic setup can impact convergence. We propose a block-diagonal SPC that has slightly more computational overhead per iteration but dramatically improves convergence of MOCCA in the spectral CT setting with three basis materials and realistic spectral responses.

We briefly summarize OSSCIR and MOCCA with  $\mu$ -preconditioning; and introduce the new block-diagonal preconditioner in Sec. II. The improvement in convergence gained by the new preconditioner is demonstrated in Sec. III on a challenging, idealized spectral CT simulation.

## II. METHODS

As in Ref. [5], the spectral CT data model is written

$$I_{w,\ell} = \int S_{w,\ell}(E) \exp \left[ - \int_{\ell} \mu(E, \vec{r}(t)) dt \right] dE, \quad (1)$$

where  $I_{w,\ell}$  is the transmitted X-ray photon fluence along ray  $\ell$  in energy window  $w$ ;  $t$  is a parameter indicating location along  $\ell$ ;  $S_{w,\ell}(E)$  is the spectral response; and  $\mu(E, \vec{r}(t))$  is the energy and spatially dependent linear X-ray attenuation coefficient.

We employ a standard material-expansion decomposition to model the attenuation map

$$\mu(E, \vec{r}(t)) = \sum_m \left( \frac{\mu_m(E)}{\rho_m} \right) \rho_m f_m(\vec{r}[t]), \quad (2)$$

where  $\rho_m$  is the density of material  $m$ ;  $\mu_m(E)/\rho_m$  is the mass attenuation coefficient of material  $m$ ; and  $f_m(\vec{r})$  is the spatial map for material  $m$ .

To obtain the final discrete data model, we combine Eq. (1) with Eq. (2); normalize the spectral response; and discretize all integrations. The standard detected counts model becomes

$$\hat{c}_{w,\ell}^{(\text{standard})}(f) = N_{w,\ell} \sum_i s_{w,\ell,i} \exp \left( - \sum_{m,k} \mu_{m,i} X_{\ell,k} f_{k,m} \right), \quad (3)$$

where  $N_{w,\ell}$  is the total number of incident photons along ray  $\ell$  in energy window  $w$ ;  $s_{w,\ell,i}$  is the normalized spectral response, i.e.  $\sum_i s_{w,\ell,i} = 1$ ;  $i$  indexes the energy  $E_i$ ;  $X_{\ell,k}$  represents X-ray projection along the ray  $\ell$ ; and  $f_{k,m}$  is the pixelized material map with  $k$  and  $m$  indexing pixel and expansion-material, respectively. The spectral responses are assumed known, and the goal is to reconstruct the material maps  $f$  from measured counts data  $c$ .

The model in Eq. (3) can cause numerical problems for IIR, because at early iterations it is possible for the sum,  $\sum_{m,k} \mu_{m,i} X_{\ell,k} f_{k,m}$ , to take on large negative values which can lead to large positive arguments for the exponential function. This issue can be remedied by imposing constraints on  $f$ , but the approach we take here is to replace the exponential function for positive arguments with a function that has slower growth; i.e. replace  $\exp(\cdot)$  with  $\text{softexp}(\cdot)$  where

$$\text{softexp}(x) = \begin{cases} \exp(x) & x \leq 0 \\ x + 1 & x > 0 \end{cases}$$

replaces the exponential function for  $x > 0$  with a linear function that matches the value and derivative at  $x = 0$ . Other cut-off points besides  $x = 0$  and extrapolations of  $\exp(x)$  are possible, but this is the form that we employ for the presented results.

The rationale for use of  $\text{softexp}(\cdot)$  is that positive arguments of  $\exp(\cdot)$  correspond to the unphysical situation that the beam intensity increases through the object; thus replacing  $\exp(\cdot)$  with  $\text{softexp}(\cdot)$  does not introduce further approximation. At the same time we avoid the need to impose constraints on  $f$ . Accordingly, the counts data model used here is

$$\hat{c}_{w,\ell}(f) = N_{w,\ell} \sum_i s_{w,\ell,i} \text{softexp} \left( - \sum_{m,k} \mu_{m,i} X_{\ell,k} f_{k,m} \right). \quad (4)$$

This modification causes a small change in the MOCCA derivation and implementation for spectral CT that was presented in Ref. [5].

*Transmission Poisson likelihood maximization:*

Maximizing the transmission Poisson likelihood is equivalent to minimizing the Kullback-Leibler distance between the counts data,  $c$ , and counts model,  $\hat{c}(f)$ ,

$$D_{\text{TPL}}(c, \hat{c}(f)) = \sum_{w,\ell} \left[ \hat{c}_{w,\ell}(f) - c_{w,\ell} - c_{w,\ell} \log \frac{\hat{c}_{w,\ell}(f)}{c_{w,\ell}} \right], \quad (5)$$

where  $c_{w,\ell}$  are the measured counts in energy window  $w$  along ray  $\ell$ . This objective function is nonconvex as can be verified by computing the Hessian (the multivariable second derivative) of  $D_{\text{TPL}}(c, \hat{c}(f))$  with respect to  $f$ . The non-linearity of  $\hat{c}(f)$  as a function of  $f$  gives rise to directions of negative curvature in  $D_{\text{TPL}}(c, \hat{c}(f))$ .

The MOCCA algorithm is designed to minimize the nonconvex  $D_{\text{TPL}}(c, \hat{c}(f))$  objective function and the pseudo-code for doing so is given in Eqs. (47)-(52) in Ref. [5]. The algorithm results from making a local convex quadratic approximation to Eq. (5). In order to form the quadratic approximation, we need to compute the first and second derivatives of

$$L_{\text{TPL}}(f) = D_{\text{TPL}}(c, \hat{c}(f)).$$

These derivatives were computed in Ref. [5], but they must be modified to account for the use of  $\text{softexp}(\cdot)$ :

$$\begin{aligned} \nabla_f L_{\text{TPL}}(f) &= Z^\top A(f)^\top r(f), \\ \nabla_f^2 L_{\text{TPL}}(f) &= -Z^\top \text{diag}(B(f)^\top r(f))Z + \\ &\quad Z^\top A(f)^\top \text{diag}(\hat{c}(f) + r(f))A(f)Z, \end{aligned}$$

where the  $w, \ell$  component of the residual  $r(f)$  is

$$r_{w,\ell}(f) = c_{w,\ell} - \hat{c}_{w,\ell}(f).$$

The component form of the matrices  $Z$ ,  $A(f)$  and  $B(f)$  are

$$\begin{aligned} Z_{\ell i, mk} &= \mu_{m,i} X_{\ell, k}, \\ A_{w\ell, \ell' i}(f) &= \frac{s_{w\ell i} \text{softexp}'[-(Zf)_{\ell i}]}{\sum_{i'} s_{w\ell i'} \text{softexp}[-(Zf)_{\ell i'}]} \mathbf{I}_{\ell \ell'}, \end{aligned} \quad (6)$$

and

$$B_{w\ell, \ell' i}(f) = \frac{s_{w\ell i} \text{softexp}''[-(Zf)_{\ell i}]}{\sum_{i'} s_{w\ell i'} \text{softexp}[-(Zf)_{\ell i'}]} \mathbf{I}_{\ell \ell'},$$

where

$$\mathbf{I}_{\ell \ell'} = \begin{cases} 1 & \ell = \ell' \\ 0 & \ell \neq \ell' \end{cases}.$$

The use of  $\text{softexp}(\cdot)$  introduces a small complication because

$$\text{softexp}''(x) \neq \text{softexp}'(x),$$

while the original MOCCA derivation made use of the fact that the first and second derivatives of  $\exp(x)$  are equal. Accordingly the first term of the Hessian  $\nabla_f^2 L_{\text{TPL}}(f)$  has the matrix  $B(f)$  instead of  $A(f)$ .

The MOCCA derivation for spectral CT relies on splitting the Hessian matrix  $\nabla_f^2 L_{\text{TPL}}(f)$  into the difference of two positive semi-definite (PSD) matrices. To accomplish this, we need to use the fact

$$\text{softexp}''(x) \leq \text{softexp}'(x), \quad (7)$$

a condition which is satisfied in our definition of  $\text{softexp}(\cdot)$ . This condition allows us to write

$$B = A - (A - B) = A - C,$$

where  $A$  and  $C$  are matrices with non-negative matrix elements. That  $C$  has non-negative matrix elements, is shown by using Eq. (7) and the fact that the spectral sensitivities  $s_{w,\ell,i}$  are non-negative. Realizing that  $B$  can be expressed as  $A - C$ , the algebra in MOCCA derivation from Ref. [5] can be followed through carrying the extra term  $-C$ . The extra term turns out to have no impact on the final pseudocode; thus the MOCCA algorithm remains the same except for the adjustment to the matrix  $A$  in Eq. (6).

For the purposes here, the salient fact is that with the various derivatives of  $L_{\text{TPL}}(f)$  computed, a convex quadrature local upperbound can be formed. In the neighborhood of an expansion point  $f_0$ , we approximate  $L_{\text{TPL}}(f)$  with

$$L_{\text{TPL}}(f) \approx Q(K(f_0)f),$$

where the precise form of the quadratic function  $Q$  is specified in Ref. [5]. The matrix  $K(f)$  is

$$K_{w\ell, mk}(f) = \sum_{\ell' i} A_{w\ell, \ell' i}(f) Z_{\ell' i, mk}.$$

The rows of  $K(f)$  index the data space consisting of energy windows,  $w$ , and rays,  $\ell$ , and the columns index the image space consisting of materials,  $m$ , and pixels,  $k$ .

*Step lengths of MOCCA and  $\mu$ -PC:* The MOCCA algorithm is primal-dual as it is based on the diagonal-SPC CPPD. Following Refs. [5,8], the step lengths for the dual and primal updates are

$$\begin{aligned} \Sigma_{w\ell} &= \frac{1/\lambda}{\sum_{m,k} |K_{w\ell, mk}(f_0)|}, \\ T_{mk} &= \frac{\lambda}{\sum_{w,\ell} |K_{w\ell, mk}(f_0)|}, \end{aligned}$$

respectively, and  $\lambda$  is a step size ratio parameter that must be tuned. In our previous work (Ref. [5]), we found that faster convergence can be obtained by applying  $\mu$ -PC to the materials basis, which transforms it to an orthogonal basis; in this new formulation of the optimization problem, the step lengths are computed the same way as before by substituting the new matrix  $K(f_0)$  calculated in this transformed basis.

*A  $m$ -block diagonal SPC for MOCCA applied to spectral CT:* The condition on  $\Sigma$  and  $T$  that leads to convergence for SPC CPPD is that the matrix

$$M = \begin{pmatrix} T^{-1} & -K^\top \\ -K & \Sigma^{-1} \end{pmatrix}$$

is positive semi-definite, i.e.  $v^\top M v \geq 0$  for any vector  $v$ . In designing step-matrices  $\Sigma$  and  $T$  for MOCCA, we respect the constraint imposed by positive definiteness of  $M$  with  $K(f_0)$  changing at each iteration.

We propose a  $m$ -block diagonal SPC for  $\Sigma$  and  $T$  that is motivated by preserving invariance to rotations of the materials expansion set; in other words, the output of the algorithm would be identical regardless of any rotation applied to the selected basis of materials, which is a natural property that is not satisfied by the  $\mu$ -PC method. In the process of developing  $\mu$ -PC we had noticed sensitive convergence behavior simply by performing such rotations. This sensitivity was traced to the diagonal PC strategy for  $\sigma$  and  $\tau$ . The proposed step matrices are

$$(\Sigma^{-1})_{w\ell, w'\ell'} = \lambda \sum_k \sqrt{\sum_m K_{w\ell, mk}^2(f_0)} \mathbf{I}_{w\ell, w'\ell'}$$

for the dual step and

$$(T^{-1})_{mk, m'k'} = \frac{1}{\lambda} \sum_{w, \ell} \frac{K_{w\ell, mk}(f_0) K_{w\ell, m'k'}(f_0)}{\sqrt{\sum_{m''} K_{w\ell, m''k}^2(f_0)}} \mathbf{I}_{k, k'},$$

for the primal step. As before, the  $\Sigma^{-1}$  matrix is diagonal, and inverting to find  $\Sigma$  only involves computing the reciprocal of the diagonal elements. The new definition of  $T^{-1}$ , however, is diagonal only in  $k, k'$  and each diagonal element indexed by  $k$  consists of an  $m \times m$  block. Inversion to find  $\Sigma$  thus involves inversion of an  $m \times m$  matrix where each entry is a  $N_k$ -length vector, where  $N_k$  is the total number of pixels in a single material map. The inversion of such an  $m \times m$  matrix is feasible, because the number of expansion materials is low. In this work in fact we use  $N_m = 3$ . The matrix inversion must be computed at every iteration because  $K(f_0)$  is a function of the expansion center, which changes at every iteration for our application

of MOCCA. The overhead in inverting the  $3 \times 3$  blocks is negligible in comparison with the computationally intensive X-ray forward- and back-projections.

### III. RESULTS

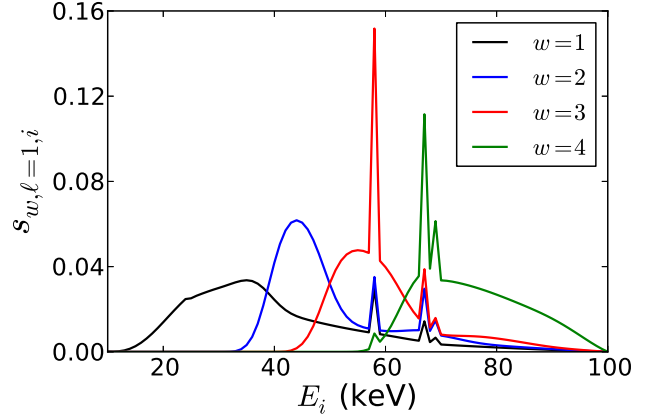


Fig. 1. Realistic X-ray normalized spectral response curves for 4-window spectral CT with a photon-counting detector. Shown is the response curves for the first detector pixel; other pixels have slight variations from these curves.

Spectral CT counts data are generated based on a simulation of our bench-top X-ray system including a photon-counting detector with 192 pixels. Mean transmitted photon counts acquired in four energy windows are computed based on spectra generated from calibration of our system. The precise spectra vary as a function of detector pixel, and example spectra are shown in Fig. 1. For the spectral CT data, 200 projections are generated from a phantom simulation of one of our physical test objects: a 6.35cm-diameter Poly(methyl methacrylate) (PMMA) cylinder with four inserted rods including PMMA, Air (empty), Teflon, and low-density polyethylene (LDPE) inserts. In the empty insert, Gd contrast agent is included at a density fraction of 0.003 (Note this is only possible in simulation). An Aluminum/PMMA/Gd materials expansion set is used for image reconstruction, and the corresponding material maps of the phantom are shown in Fig. 2.

The test data are the noiseless mean counts, and the goal of this “inverse crime” set up is to characterize MOCCA convergence for  $\mu$ -PC and  $m$ -block diagonal SPC by observing the accurate recovery of the test object. The difficulty of the problem lies in the fact that we employ realistic spectra that include non-flux-dependent physical factors that blur the sharp energy-window borders. The blurred spectra have realistic

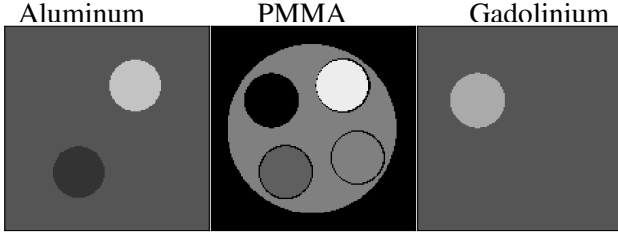


Fig. 2. Rods phantom decomposed into Aluminum, PMMA, and Gd maps. The structure of the phantom is most easily visible in the PMMA map, where the PMMA background cylinder is clearly visible. The rods, clockwise from the upper left are: Gd at a density fraction of 0.003, Teflon, PMMA, and LDPE. The Gd "rod" is only visible in the Gd map. The display windows are  $[-0.1, 0.2]$ ,  $[0.5, 1.5]$ , and  $[-0.003, 0.006]$  for Aluminum, PMMA, and Gd maps, respectively.

overlap with each other as opposed to ideal spectral responses with no overlap.

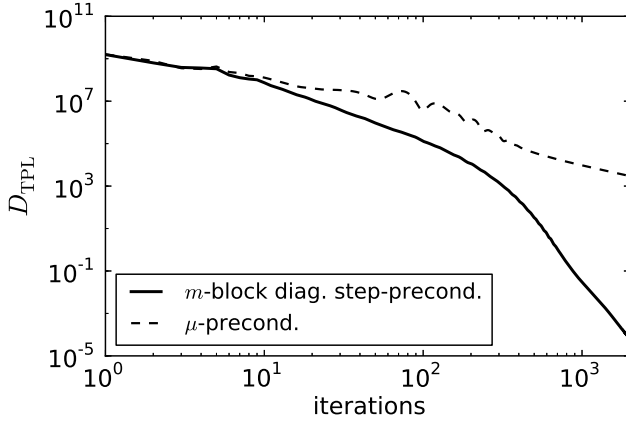


Fig. 3. The log-log plot shows convergence of  $D_{\text{TPL}}(c, \hat{c}(f^{(n)}))$ , where  $f^{(n)}$  is the material map estimates at iteration  $n$ . The curves show results for MOCCA with  $\mu$ -PC and with  $m$ -block diagonal SPC.

In Fig. 3, we display the  $D_{\text{TPL}}$  data discrepancy as a function of iteration number for both PC strategies. In each case the  $\lambda$  parameter is tuned for most rapid convergence in this quantity. Both versions of MOCCA are run for 2,000 iterations and in this example it is clear that  $m$ -block diagonal SPC outperforms  $\mu$ -PC. Not shown is the result for MOCCA with diagonal SPC, which exhibits divergent behavior for all tested  $\lambda$  values. Divergent behavior can occur with MOCCA, when only a single "inner loop" is performed [4,5]. Due to efficiency constraints, we aim to operate MOCCA with parameter and preconditioning choices that allow its operation without nested inner and outer loops.

Of particular interest for convergence studies, in this case, is the Gd material map. It has such low density

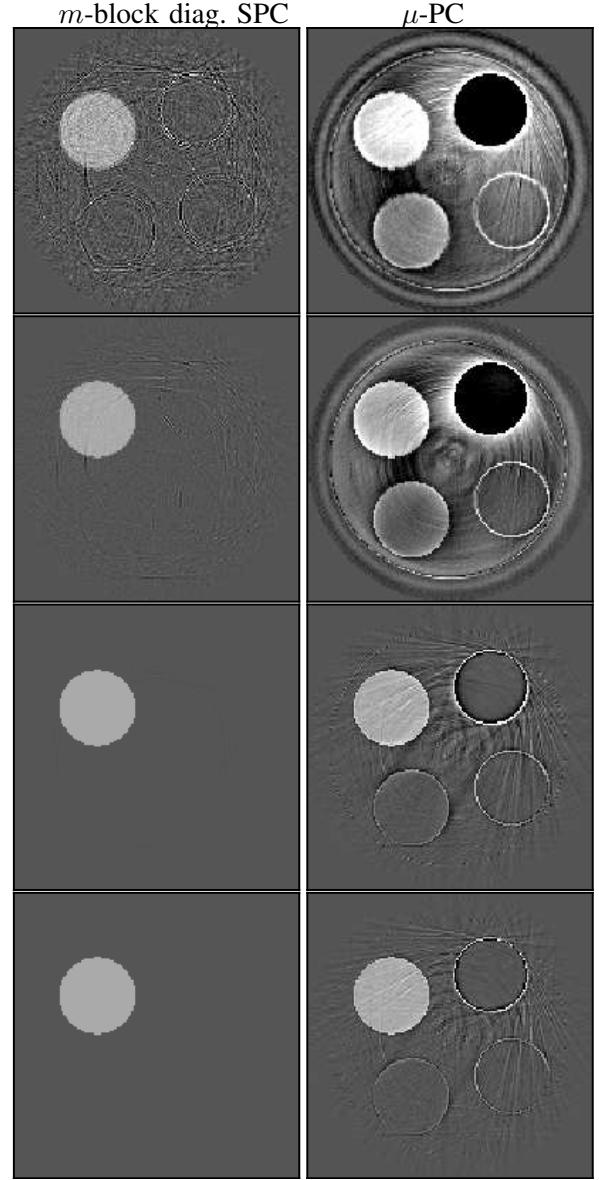


Fig. 4. Gd material maps at various iteration numbers for MOCCA with the new  $m$ -block diagonal SPC and with  $\mu$ -PC. From top to bottom the iteration numbers are: 100, 200, 1000, and 2000. The display window is  $[-0.003, 0.006]$  for all panels.

that lack of convergence is obvious in visualizing the corresponding images. In Fig. 4, we display a series of intermediate estimates of the Gd map for both pre-conditioning methods. Of particular interest is the fact that at 100 iterations the proposed  $m$ -block method has little contamination from the PMMA and aluminum maps, while  $\mu$ -PC shows significant bleed-through from the other expansion materials at 100 and 200 iterations. From the images series it is also clear that the  $m$ -block method achieves accurate Gd recovery much earlier than  $\mu$ -PC. We also note that the artifact patterns are rather complex at intermediate iterations;

this results from the variations of spectral response across detector pixels.

#### IV. SUMMARY

We propose a new  $m$ -block diagonal step-preconditioner for use with MOCCA applied to spectral CT. In these preliminary convergence studies we have primarily been concerned with K-edge imaging with the use of a three-material expansion set: a soft-tissue equivalent, a bone equivalent, and Gd contrast agent. In this setting, the new preconditioner enables MOCCA to be applied effectively for one-step reconstruction of three three material maps from four-window photon-counting data with realistic spectral responses. At the conference, we will also present experimental results on our K-edge imaging phantom using MOCCA with  $m$ -block diagonal step-preconditioning.

#### V. ACKNOWLEDGMENT

RFB is supported by an Alfred P. Sloan Fellowship and by NSF award DMS-1654076. This work is also supported in part by NIH Grant Nos. R01-EB018102, and R01-CA182264. The contents of this article are solely the responsibility of the authors and do not necessarily represent the official views of the National Institutes of Health.

#### REFERENCES

- [1] J. P. Schlomka, E. Roessl, R. Dorscheid, S. Dill, G. Martens, T. Istel, C. Bäumer, C. Herrmann, R. Steadman, G. G. Zeitler, A. Livne, and R. Proksa, "Experimental feasibility of multi-energy photon-counting K-edge imaging in pre-clinical computed tomography," *Phys. Med. Biol.*, vol. 53, no. 15, pp. 4031–4048, 2008.
- [2] T. G. Schmidt, R. F. Barber, and E. Y. Sidky, "A spectral ct method to directly estimate basis material maps from experimental photon-counting data," *IEEE Trans. Med. Imag.*, pp. 1808–1819, 2017.
- [3] B. Chen, Z. Zhang, E. Y. Sidky, D. Xia, and X. Pan, "Image reconstruction and scan configurations enabled by optimization-based algorithms in multispectral CT," *Phys. Med. Biol.*, vol. 62, pp. 8763–8793, 2017.
- [4] R. F. Barber and E. Y. Sidky, "MOCCA: mirrored convex/concave optimization for nonconvex composite functions," *J. Mach. Learn. Res.*, vol. 17, no. 144, pp. 1–51, 2016.
- [5] R. F. Barber, E. Y. Sidky, T. Gilat-Schmidt, and X. Pan, "An algorithm for constrained one-step inversion of spectral CT data," *Phys. Med. Biol.*, vol. 61, pp. 3784–3818, 2016.
- [6] A. Chambolle and T. Pock, "A first-order primal-dual algorithm for convex problems with applications to imaging," *J. Math. Imag. Vis.*, vol. 40, pp. 120–145, 2011.
- [7] E. Y. Sidky, J. H. Jørgensen, and X. Pan, "Convex optimization problem prototyping for image reconstruction in computed tomography with the Chambolle-Pock algorithm," *Phys. Med. Biol.*, vol. 57, pp. 3065–3091, 2012.
- [8] T. Pock and A. Chambolle, "Diagonal preconditioning for first order primal-dual algorithms in convex optimization," in *2011 IEEE International Conference on Computer Vision (ICCV)*, 2011, pp. 1762–1769.